Proceedings of The National Conference
On Undergraduate Research (NCUR) 2018
University of Central Oklahoma, OK
Edmond, Oklahoma
April 5-8, 2018

Designing And Optimizing Silicon Waveguides For Integration With Non-Linear Optics

Peter Shares
Department of Electrical Engineering and Computer Science
United States Military Academy
West Point, NY 10996

Faculty Advisors: Dr. Kirk Ingold

Abstract

Second-order nonlinear optics are used in a wide variety of applications such as second harmonic frequency generation. One nonlinear crystal, lithium niobate ($LiNbO_3$ or LN), has shown to be highly efficient for visible and infrared (IR) wavelength conversions. Established techniques exist to fabricate LN into varying waveguide designs, however, the bulk form is limited for small-scale mid-IR applications. Silicon (Si) fabrication processes for nanoscale photonic applications are well developed yet do not exhibit the level of second-order nonlinearities of LN. This research investigates combining these two processes to take advantage of the waveguide fabrication techniques for silicon and the large second order nonlinearity of LN. Assuming LN bonded to a Si waveguide, the goal of this research was to optimize the dimensions of the waveguide to maximize the mode coupling of mid-IR light between the LN and Si. All designs were simulated with commercial software using finite element simulation and finite difference time domain methods. Two designs were investigated to optimize the mode overlap of a pump and secondary beam intended for second harmonic generation. The first utilized thin-film LN bonded to a Si-waveguide fabricated on silicon-on-insulator. Although this technique achieved as much as 50% mode overlap, the large absorption coefficient of silicon dioxide (SiO_2) insulator has a negative effect on mid-IR wavelengths. The alternative design used a Si-waveguide bonded to bulk LN. This design was not limited by the absorption of the SiO_2, however the maximum mode overlap was limited to less than 30%.

Keywords: Non-linear Optics, Lithium Niobate, Silicon Photonics

1. Background and Motivation

Bulk non-linear optics offer a wide range of applications for photonics research. More specifically, periodically-poled Lithium Niobate ($LiNbO_3$ or LN) is often used for its high nonlinear coefficient ($\chi^{(2)}$) in applications such as electro-optic modulators and wavelength conversion devices.[1,2] In particular, for the latter, LN is attractive for wavelengths in the mid-infrared (IR) range. However, in most cases these applications use free-space cavities that can be several meters in length, limiting the overall scalability.[3,4] Recent work has shown different methods of reducing the size of LN-based wavelength conversion applications, to include nanophotonic LN waveguides and silicon/LN integrated devices.[5,6] An attractive quality of the latter, is that silicon photonics offers mature fabrication process for creating nanoscale resonators.

The work presented here seeks to expand upon research combining the fabrication of silicon waveguides with the high nonlinearity of lithium niobate using an approach similar to work by Weigel, et al., however focused on wavelengths extending into the mid-infrared (>3μm).[7] This approach involves using commercial simulation software to identify supported optical modes based on near-infrared and mid-infrared wavelengths for various waveguide dimensions. All of the work presented here assumes a lithium niobate wafer bonded to a silicon-on-insulator wafer.

Previous work has shown the potential for patterning silicon waveguides on both thin-film LN and bulk LN wafers.[8,9] These two processes are assumed for the different simulation results shown here.

Overall, this experiment seeks to determine the feasibility of integrating silicon photonics with bulk and thin-film non-linear optics for the purpose of second harmonic generation (SHG) at wavelengths in the mid-infrared range (~2-4 μm). Second harmonic generation of a wavelength will reduce the fundamental, or pump, wavelength by a factor of two, thereby doubling the frequency of the light as described in Equations 1 and 2.[10]

$$\frac{dE(\omega)}{dz} = i\kappa E(2\omega)E^*(\omega)e^{i\Delta kz} \tag{1}$$

$$\frac{dE(2\omega)}{dz} = i\kappa E(\omega)E(\omega)e^{-i\Delta kz} \tag{2}$$

The commercial software, Synopsis® RSoft software is used for all simulations. Initially, the finite element mode solver, FemSIM™, is used to determine the mode profiles at the pump and SHG wavelengths. These modes are then used in the finite-difference time-domain software, FullWAVE™, to simulate the propagation of the light through the waveguide. For the purpose of this work, the pump wavelength is 4.18μm and the SHG wavelength is 2.09μm. The light is assumed to be in the TE-polarization.

2. Simulation Setup and Methodology

To design the silicon waveguide, the parameters of the waveguide, in particular the width and height, were varied while keeping the lithium niobate and silicon dioxide dimensions constant. Similar to the work by Weigel, et al., the design goal here was to determine the waveguide dimensions that would support a mode transition between the silicon waveguide and the lithium niobate. Schematics of the two designs are shown in Figure 1.

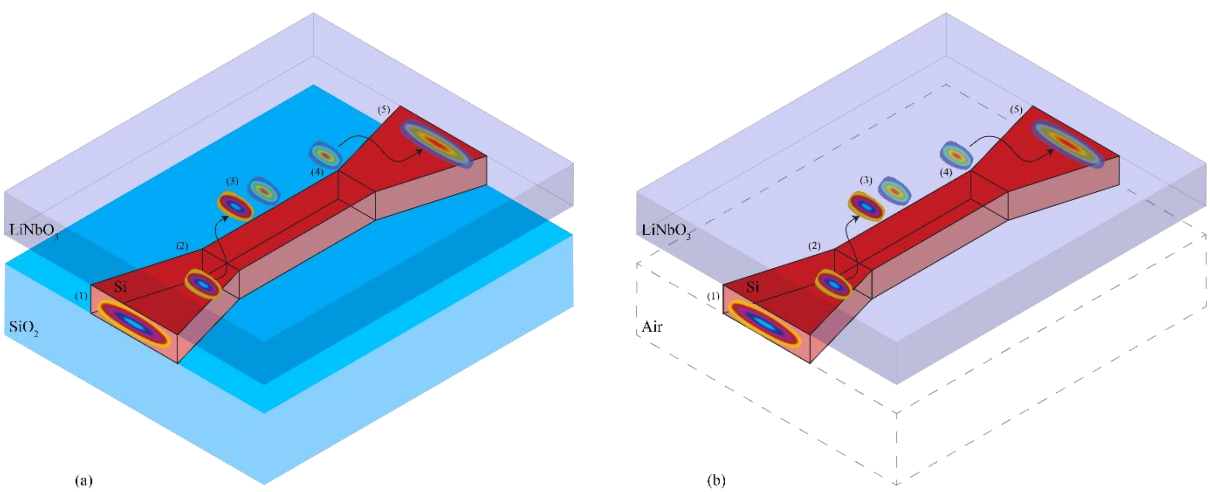

Figure 1. Concept for the silicon waveguide and lithium niobate SHG devices. (a) Thin film LN on oxide with silicon oxide. The oxide layers are maintained on the top and bottom of the device. (b) Bulk LN with the oxide layer etched off to keep an air cladding on the bottom of the device.

The first design uses a thin-film lithium niobate on oxide (h_{LN} < 1μm) shown in Figure 1(a) and maintains the oxide layer of the silicon waveguide. For visual appearance, the oxide layer on top of the LN is not shown. Additional silicon bonding surfaces would be used to facilitate a solid bond between the silicon and lithium niobite.[7] In actual practice, the lower oxide layer could be etched off to provide an air cladding. For the purpose of this work, this was not considered. For these simulations, h_{LN} = 1μm. Figure 1(b) shows the design using a bulk lithium niobate (h_{LN} ~ 0.5 – 1mm). The advantage of the second design is in the lack of the oxide layer. Silicon dioxide is highly absorptive

in the mid-infrared, at wavelengths greater than 3.5μm.[11] This design uses an air cladding to confine the mode to the silicon and lithium niobate, respectively. For these simulations, h_{LN} = 500μm.

Figure 1 also shows the concept of the mode coupling. At point (1), the mode is completely coupled into the silicon waveguide. An adiabatic taper is used to reduce the silicon waveguide such that at point (2) the mode is coupled from the silicon to the LN. Based on Equations (1) and (2), it is assumed the fundamental beam generates the second harmonic in the LN as shown at point (3). At point (4), the SHG mode is still primarily in the LN. With another adiabatic taper, the silicon waveguide width is increased to couple the SHG mode into the waveguide, as shown at point (5).

Figure 2 shows the cross sections of both designs. Initially, modes supported in both the waveguide and the lithium niobate were determined using the FemSIM™ mode solver at the pump and SHG wavelengths. The height of the silicon, h_{Si}, was set and then the waveguide width, w_{Si}, was optimized to support modes for both the pump and SHG wavelengths. These modes were then used as launch parameters for the FullWAVE™ simulator to investigate the propagation of the light through the devices.

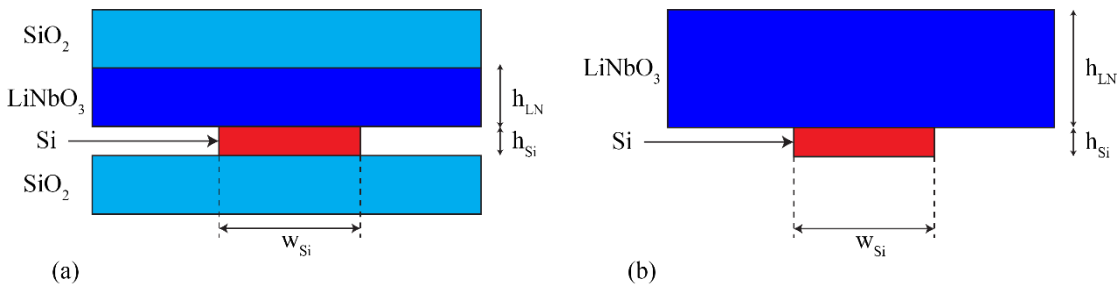

Figure 2. Cross sections of the two simulated designs: (a) thin-film lithium niobate with the oxide, SiO_2, layers and (b) bulk lithium niobate with air cladding.

3. Results

The following shows the results of the various simulations performed in RSoft. With a fixed waveguide height, h_{Si} = 0.27μm, the partial power within the waveguide and the lithium niobate for the thin-film LN design is shown in Figure 3(a) for a scan of the waveguide width at the pump and SHG wavelengths. A similar scan is shown in Figure 3(b) for the bulk LN design.

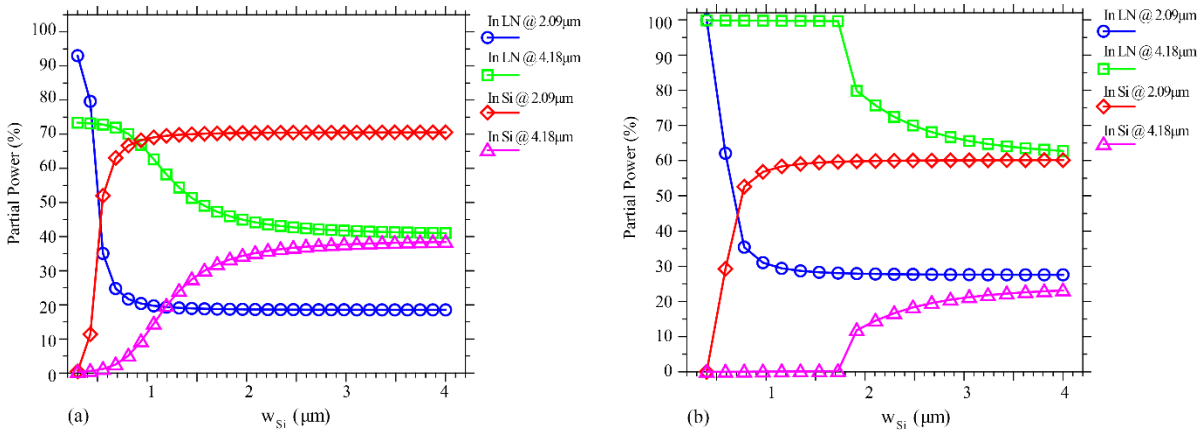

Figure 3. (a) Thin-film LN design and (b) Bulk LN design. For both designs, as the waveguide width, w_{Si}, increases, the partial power of the beam is coupled from the silicon waveguide to the LN.

For the thin-film LN design, the optimal width to couple both the fundamental and SHG wavelengths into the LN is 1μm. At this width, roughly 20% of the fundamental mode and 66% of the SHG mode is coupled into the LN. Although the amount of couple power seems low for the SHG, below a width of 1μm the fundamental mode is not confined as well. The mode profiles for this design is shown in Figure 4. For the bulk LN design, the optimal width

is 2μm. This couples roughly 28% of the fundamental mode and 75% of the SHG mode into the LN. Mode profiles are shown in Figure 5. The cross section of these images corresponds to those in Figure 2 for the thin-film and bulk designs.

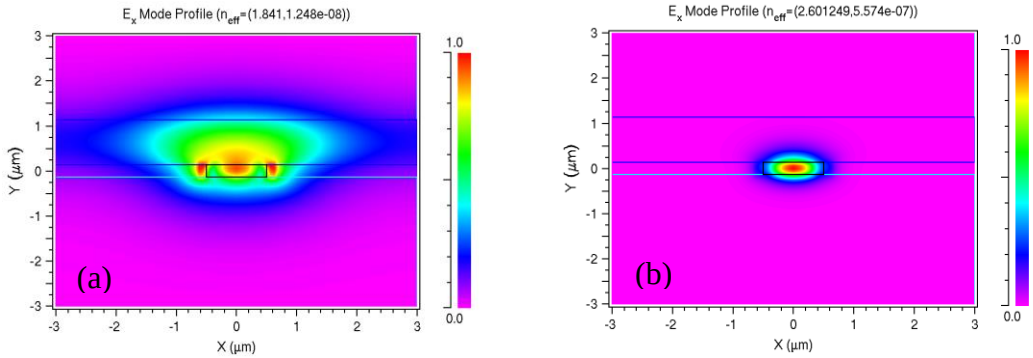

Figure 4. Mode profiles for the thin-film LN design with a waveguide with of 1μm. (a) At 4.18μm, 65% of the mode is contained in the LN. (b) At 2.09μm, 20% of the mode is contained in the LN.

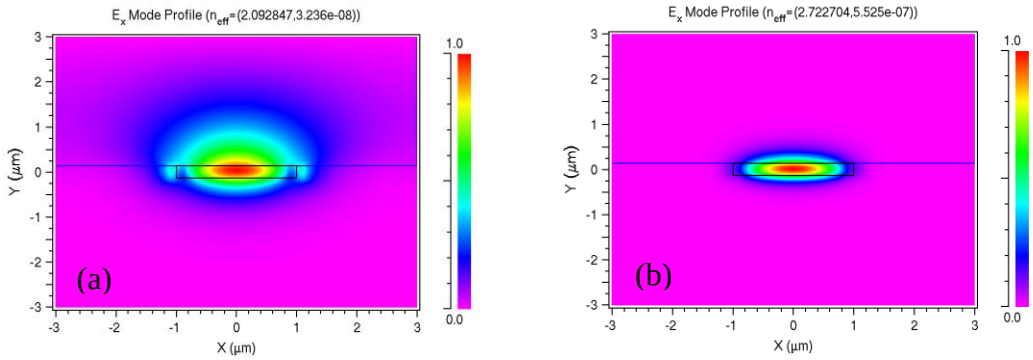

Figure 5. Mode profiles for the bulk LN design with a waveguide with of 2μm. (a) At 4.18μm, 58% of the mode is contained in the LN. (b) At 2.09μm, 20% of the mode is contained in the LN.

These fundamental mode profiles were then used as the launch parameters in the FullWAVE™ method to simulate the propagation of the mode through a 150μm adiabatic taper. For the taper, the large width of the taper was set to 4μm for both designs. As shown in Figure 6, as the fundamental mode propagated along the taper in the *z*-direction, the mode transitioned from the silicon waveguide into the LN. Similar results were obtained for the bulk LN design. These results are shown in Figure 7. It is apparent in the *yz*-plane of the bulk LN design, the percentage of the fundamental mode in the LN is lower than that of the thin-film LN design. However, both designs show a good transition between the waveguide and the LN.

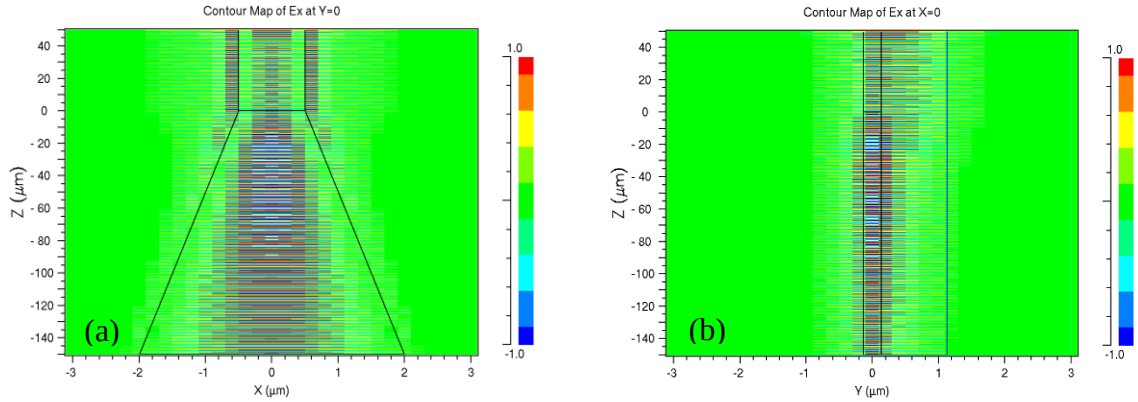

Figure 6. FullWAVE™ results for the thin-film LN design of the fundamental mode propagating in the *z*-direction. (a) The *xz*-plane showing the fundamental mode decreasing along the taper. (b) The *yz*-plane showing the transition of the fundamental mode from the silicon waveguide into the LN.

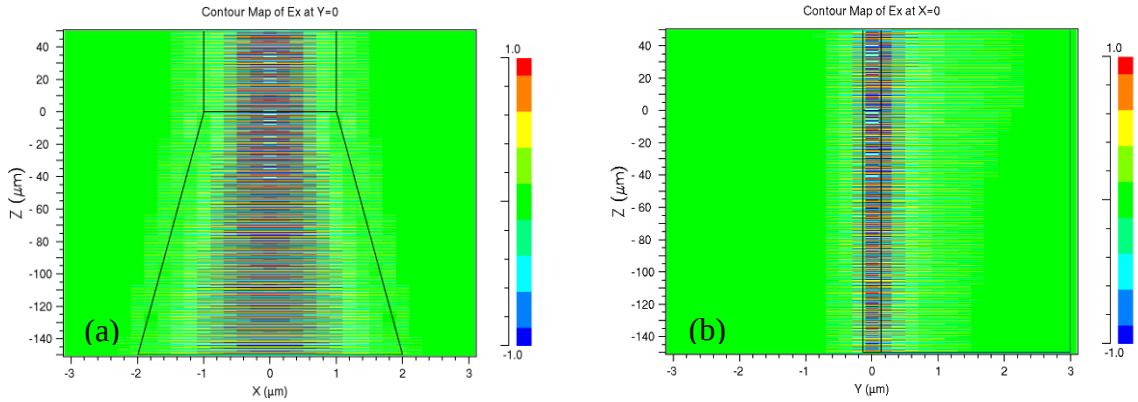

Figure 7. FullWAVE™ results for the bulk LN of the fundamental mode propagating in the *z*-direction. (a) The *xz*-plane showing the fundamental mode decreasing along the taper. (b) The *yz*-plane showing the transition of the fundamental mode from the silicon waveguide into the LN.

Following the transition of the fundamental mode from the waveguide into the LN and assuming the generation of the SHG mode according to Figures 4(b) and 5(b), similar simulations were run to show the transition of the SHG mode from the LN back into the waveguide. The results are shown in Figures 8 and 9 for the thin-film and bulk designs, respectively. It is apparent the SHG mode expands with the taper. Additionally, as the taper grows, the SHG mode becomes more confined to the waveguide, as expected. These results show that the SHG signal can be manipulated such that more complex waveguide designs, such as resonators, could be implemented with the bonded LN.

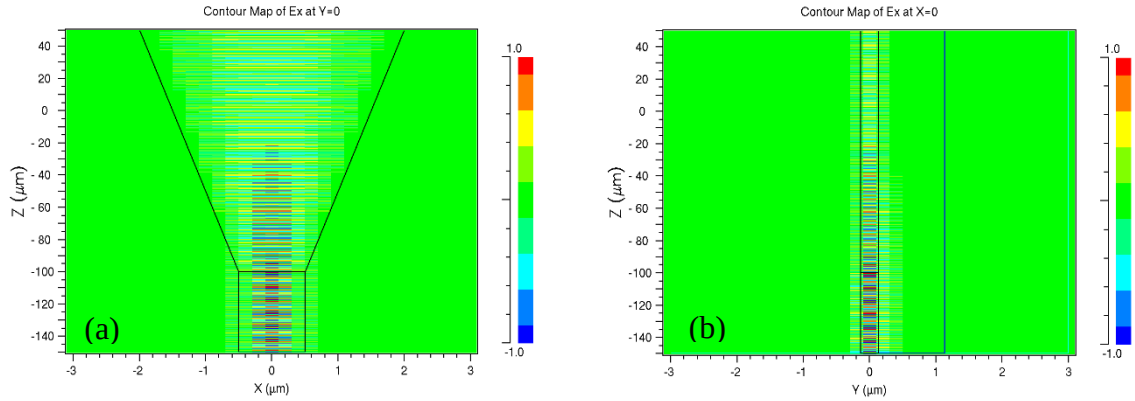

Figure 8. FullWAVE™ results for the thin-film LN design of the SHG mode propagating in the *z*-direction. (a) The *xz*-plane showing the SHG mode increasing along the taper. (b) The *yz*-plane showing the transition of the SHG mode from the LN into the silicon waveguide.

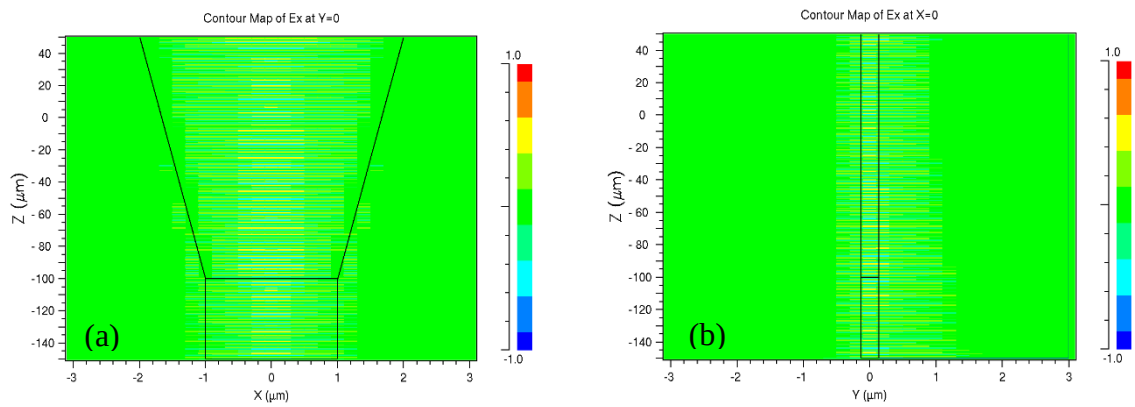

Figure 9. FullWAVE™ results for the bulk LN design of the SHG mode propagating in the *z*-direction. (a) The *xz*-plane showing the SHG mode increasing along the taper. (b) The *yz*-plane showing the transition of the SHG mode from the LN into the silicon waveguide.

The results show good agreement with the mode solver and that the fundamental and SHG modes couple in and out of the LN and the silicon waveguide. One major assumption for these simulations is that the SHG mode generated according the Equations 1 and 2 would be identical to the supported mode shown in Figures 4(b) and 5(b). In actuality, the SHG mode would have a mode profile similar to the fundamental mode, however reduced by a factor of $\sqrt{2}$.[12] To account for this, the mode overlap of the fundamental and SHG modes, accounting for the reduction factor were calculated. The following mode overlap integral was used[13]

$$\eta = \frac{\left|\iint E_{pump}(x,y) E_{SHG}^{*}(x,y)\, dx\, dy\right|^2}{\iint \left|E_{pump}(x,y)\right|^2 dx\, dy \iint \left|E_{SHG}(x,y)\right|^2 dx\, dy}. \tag{3}$$

Using MATLAB and the generated mode profiles, Equation 3 resulted in roughly 30% mode overlap of the fundamental and SHG modes for both designs. This suggests both designs would be feasible for generating the second harmonic of the fundamental.

The absorption of the fundamental mid-infrared mode has been neglected. It is important to highlight that in the thin-film LN design, as much as 10-15% of the fundamental mode is coupled into the oxide layer. Due to the high absorption at the fundamental wavelength, this could result in a reduced overall SHG efficiency. Whereas the thin-film LN design has simpler fabrication steps, it comes at the cost of a potential reduction in efficiency.

5. Future Work

The next step in this research would be to fabricate both waveguide designs. Further work is required to fully design a device that could be tested. As an example, coupling light into the waveguide would require some mode adapter. In particular, due to the mid-infrared wavelength, a grating coupler may be the best option. This would require additional design and simulations to determine the appropriate grating period and dimensions. This would also likely reduce the overall efficiency.

6. Acknowledgements

The author acknowledges the Army Research Office and the Department of Electrical Engineering & Computer Science at the United States Military Academy, West Point, NY for funding this project, and Columbia University for allowing the author to utilize their RSoft license for the simulations.

7. References

1. E. L. Wooten, K. M Kissa, A. Yi-Yan, E. J. Murphy, D. A. Lafaw, P. F. Hallemeier, D. Maack, D. V. Attanasio, D. J. Fritz, G. J. McBrien, and D. E. Bossi, “A review of lithium niobate modulators for fiber-optic communications systems,” IEEE J. Sel. Top. Quant. 6(1), 69-82 (2000).
2. Robert Boyd, Nonlinear Optics (California: Elsevier Press, 2003), 4-13.
3. K. A. Ingold, A. Marandi, C. W. Rudy, K. L. Vodopyanov, and R. L. Byer, “Fractional-length sync-pumped degenerate optical parametric oscillator for 500-MHz 3-μm mid-infrared frequency comb generation,” Opt. Lett. 39, 900-903 (2014).
4. A. Marandi, N. C. Leindecker, K. L. Vodopyanov, and R. L. Byer, “All-optical quantum random bit generation from intrinsically binary phase of parametric oscillators,” Opt. Express 20, 19322-19330 (2012).
5. C. Wang, C. Langrock, A. Marandi, M. Jankowski, M. Zhang, B. Desiatov, M. M. Fejer, and M. Lončar, “Second-harmonic generation in nanophotonic PPLN waveguides with ultrahigh efficiencies,” in Conference on Lasers and Electro-Optics, OSA Technical Digest (online) (Optical Society of America, 2018), paper JTh5A.2.
6. A. Rao, M. Malinowski, A. Honardoost, J. R. Talukder, P. Rabiei, P. Delfyett, and S. Fathpour, “Second-harmonic generation in periodically-poled thin film lithium niobate wafer-bonded on silicon,” Opt. Express 24, 29941-29947 (2016).
7. Peter O. Weigel, Marc Savanier, Christopher T. DeRose, Andrew T. Pomerene, Andrew L. Starbuck, Anthony L. Lentine, Vincent Stenger, Shayan Mookherjea, “Lightwave Circuits in Lithium Niobate through Hybrid Waveguides with Silicon Photonics”, Sci. Rep. 6, 22301 (2016).
8. J. Chiles and S. Fathpour, “Mid-infrared integrated waveguide modulators based on silicon-on-lithium-niobate photonics,” Optica 1, 350-355 (2014).
9. A. Rao, et al, “Second-harmonic generation in periodically-poled thin film lithium niobate wafer-bonded on silicon.”
10. R. L. Byer, Parametric Oscillators and Nonlinear Materials (Academic Press, New York, 1977), p. 60.
11. S. A. Miller, M. Yu, X. Ji, A. G. Griffith, J. Cardenas, A. L. Gaeta, and M. Lipson, "Low-loss silicon platform for broadband mid-infrared photonics," Optica 4, 707-712 (2017).
12. R. L. Byer, Parametric Oscillators and Nonlinear Materials, p.72.
13. Gerd Keiser, “Optical Fiber Communications.” 4th ed. New York, NY: McGraw-Hill Companies, 2011.